

Dynamical real-space renormalization group calculations with a new clustering scheme on random networks

D. Balcan¹ and A. Erzan^{1,2}

¹ *Department of Physics, Faculty of Sciences and Letters*

Istanbul Technical University, Maslak 34469, Istanbul, Turkey

² *Gürsey Institute, P.O.B. 6, Çengelköy, 34680 Istanbul, Turkey*

(Dated: November 23, 2018)

We have defined a new type of clustering scheme preserving the connectivity of the nodes in network ignored by the conventional Migdal-Kadanoff bond moving process. Our new clustering scheme performs much better for correlation length and dynamical critical exponents in high dimensions, where the conventional Migdal-Kadanoff bond moving scheme breaks down. In two and three dimensions we find the dynamical critical exponents for the kinetic Ising Model to be $z = 2.13$ and $z = 2.09$, respectively at pure Ising fixed point. These values are in very good agreement with recent Monte Carlo results. We investigate the phase diagram and the critical behaviour for randomly bond diluted lattices in $d=2$ and 3, in the light of this new transformation. We also provide exact correlation exponent and dynamical critical exponent values on hierarchical lattices with power-law degree distributions, both in the pure and random cases.

PACS. 05.50.+q, 64.60.-i

I. INTRODUCTION

We have generalized the dynamical real-space renormalization group (RSRG) calculations for the kinetic Ising model [1] to dilute lattices with arbitrary number of nearest neighbors, motivated by an interest in the relaxation behaviour on networks [2] with scale free and exponential degree distributions.

We first computed the dynamical critical exponent z , in the Migdal-Kadanoff bond moving scheme [3, 4] on networks with arbitrarily high, but uniform, connectivity and found as have others [5, 6], that z gradually converges to unity, as the spatial dimension of the system becomes very large (for $d = 12$, $z - 1 = 10^{-5}$), and the correlation length exponent converges to $\nu = 1$. (See Fig. 1 and 2) This is in contrast to the expected Mean Field values of $\nu = 0.5$ and $z = 2$ above the upper critical dimension. The dynamic real-space renormalization group calculation thus yields neither a sharp crossover above the upper critical dimension, $d_c=4$, nor the correct Mean Field behaviour in the high dimension limit. We have observed that a static RSRG calculation with Migdal-Kadanoff bond moving scheme (MK) also converges to the same limits, but it does so from above, whereas the dynamical RSRG calculation does so from below. (See Fig. 2)

The reason why the MK approach fails to provide a reasonable approximation to the critical behaviour of d dimensional hypercubic lattices in large d , is twofold. The first is because it underestimates the contribution from the loops in the d -dimensional Euclidean lattice and this effect leads to more and more inaccurate results for large dimensions. We have found a way to improve the performance of the RS approach in relation to d -dimensional hypercubic lattices, by defining a new type of RSRG cluster, which retains the inter-connectivity of the moved spins, and were able to obtain a convergence to $\nu = 0.63$ (better than 1 but still larger than 0.5) in

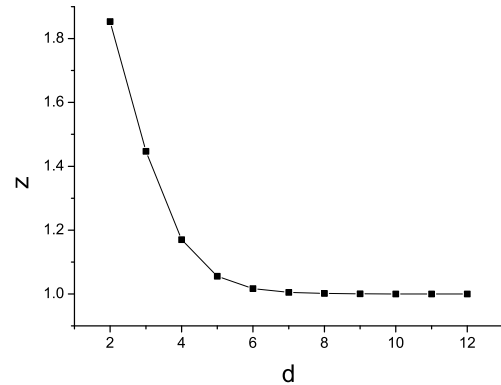


FIG. 1: The dynamical critical exponent z versus dimension d obtained via the conventional Migdal-Kadanoff bond moving scheme. z converges to 1 for large d .

the limit of large dimensionality ($d > 13$). (See Fig. 3) Likewise, the dynamical critical exponent in this scheme converges to the value 1.6 for dimensions $d \geq 11$. (See Fig. 4) The new clustering scheme for the RSRG also performs very well in low dimensions. The dynamical exponent calculated within our scheme for $d = 2$ is $z = 2.13$ and for $d = 3$ is $z = 2.09$, to be compared with the best simulation results [7, 8, 9, 10, 11, 12, 13], which give values between 2.11 and 2.24 for $d = 2$ and between 2.01 and 2.11 for $d = 3$.

The second reason for the divergence of MK results from those on Euclidean hypercubic lattices, is the nonuniform topology of the underlying hierarchical lattice, on which the MK scheme for RSRG is realised as an exact transformation. [14, 15] We turn this feature to an advantage in investigating the dynamical behaviour of the Ising model on networks with power-law degree distributions.

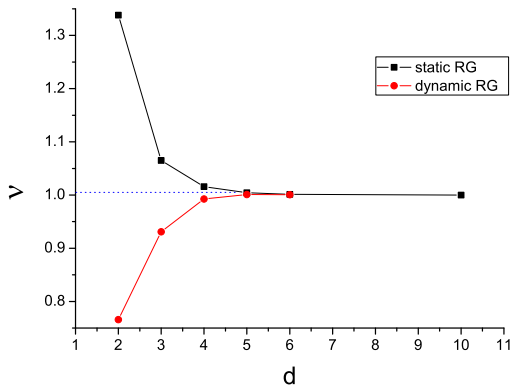


FIG. 2: The correlation critical exponent ν versus dimension d via the conventional Migdal-Kadanoff bond moving scheme. ν converges to 1 for large d .

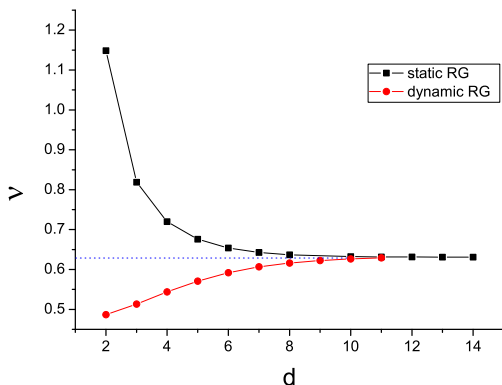


FIG. 3: The correlation critical exponent ν versus dimension d obtained by our new clustering scheme. ν converges to 0.63 for large d (compare it with Fig. 2).

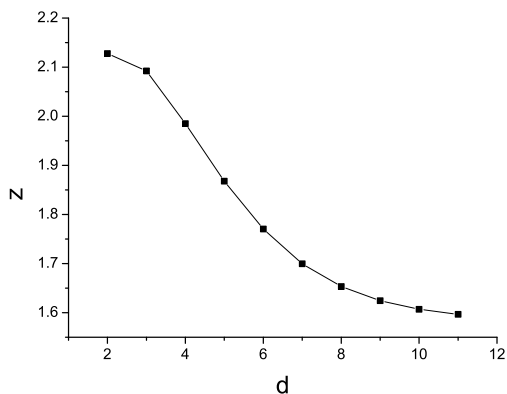


FIG. 4: The dynamical critical exponent z versus dimension d obtained by our new clustering scheme. z converges to 1.6 for large d (compare it with Fig. 1).

Going over to the dynamical critical behaviour for bond diluted lattices, we first applied the dynamic RSRG technique to the bond diluted kinetic Ising system in two and three dimensions. The approximation we used to compute the configuration averages is in fact exact for annealed randomness. The approximate transformations for the dilution parameter p and the coupling constant are well behaved as one approaches the separatrix, or critical line, from above, but the approximation breaks down in the ordered phase and for low temperatures in the disordered phase. In both two and three dimensions we were able to compute the RG flows on the disordered side of the separatrix and on the separatrix itself, and thereby determine the phase diagrams. In two dimensions we find a disorder fixed point, which is unstable, and which we interpret as a tricritical point, since there the second order phase transition line gives way to a first order transition line. The pure Ising fixed point is stable, and determines the exponents along the second order transition line. In three dimensions, no disordered critical fixed point is found. The critical line is depressed to zero temperature at a concentration $p_e > p^*$, where p^* is the percolation fixed point. The flow along the critical line is to the pure Ising fixed point at $p = 1$, and thus the critical exponents along the critical line are the same as the pure Ising exponents, also in three dimensions. Computing the effective critical exponents along the critical line, we find that z_{eff} varies non-monotonically as a function of p , within the intervals $[2.01, 2.25]$ for $d = 2$ and $[2.09, 2.69]$ for $d = 3$.

Our scheme as well as the conventional equilibrium Migdal-Kadanoff RSRG (see also Ref. [16, 17]) fails to predict the crossover to a disorder critical fixed point for $d = 3$, both demonstrated by means of finite size scaling arguments [18] applied to large Monte Carlo simulations [19] and expected on the basis of the Harris criterion [20]. The value we find for the pure system specific heat exponent α via the hyper-scaling relation $2 - \alpha = d\nu$ in $d = 3$ is negative for the static RSRG calculation for ν , while the dynamic calculation yields a positive α . These results have to be interpreted in the context of the still ongoing debate on the criteria for the stability of the pure-system critical behaviour. The rather extensive literature on the Harris criterion [20] has been recently reviewed by Janke and Weigel [21]. It has been shown by various authors [17, 22, 23] that the Harris criterion, which equates the crossover exponent for randomness, ϕ to the pure system α , is simply not applicable on hierarchical lattices, and various alternative criteria, such as the “wandering exponent” [22] for correlations in the non-periodic variations in the number of bonds incident on lattice points (the degree of the node) have been proposed. The calculation of this exponent for our present RSRG scheme goes beyond the scope of this paper and will be considered in a separate publication.

The paper is organized as follows. In the next section we setup the dynamical RSRG calculations for bond diluted hypercubic lattices, and introduce a new clustering

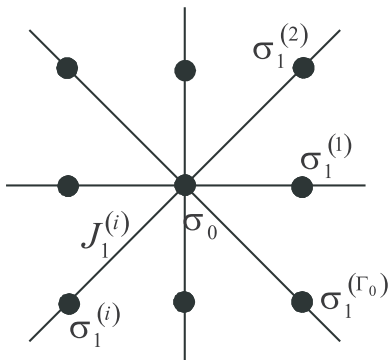


FIG. 5: The “central” spin on which we concentrate is denoted by σ_0 , its nearest neighbor spins by $\sigma_1^{(i)}$, and the interaction constants by $J_1^{(i)}$, where i takes values from 1 to Γ_0 .

scheme on which we will implement it. The last section includes our results and a discussion of the relevance of our results to non-uniform lattices with power law degree distributions.

II. THE DYNAMICAL RSRG CALCULATIONS FOR BOND DILUTED HYPERCUBIC LATTICES

In order to investigate the effect of the underlying lattice of arbitrarily high degree on dynamical behaviour of an interacting system living on this lattice, we consider an Ising model on the nodes of a hypercubic lattice of d -dimensions, which will be subjected to bond dilution to yield a random network with a Poisson degree distribution.

The hamiltonian of the system is given by

$$H = - \sum_{\langle ij \rangle} J_{ij} \sigma_i \sigma_j, \quad (1)$$

where J_{ij} is the interaction between two nearest neighbor spins and σ_i is the spin variable which can take the values $+1$ and -1 . The sum is taken over all nearest neighbor pairs. In a d -dimensional hypercubic lattice the maximum number of nearest neighbor spins with a nonzero interaction is $\Gamma_0 = 2d$. Now we will concentrate on a spin and its neighborhood: we will denote this spin by σ_0 , the nearest neighbor spins and the interaction constants by $\sigma_1^{(i)}$ and $J_1^{(i)}$, respectively, where i takes values from 1 to Γ_0 as shown in Fig. 5. Here $J_1^{(i)}$ is subjected to the distribution,

$$P(J_1^{(i)}) = p\delta(J_1^{(i)} - J) + (1-p)\delta(J_1^{(i)}). \quad (2)$$

A. Equation of motion for the magnetization

Using Glauber dynamics [24] we may write down the equation of motion for the magnetization $m_0 \equiv \langle \sigma_0 \rangle$ and

get

$$\frac{d}{dt} m_0(t) = -m_0(t) + \langle \tanh \left(\sum_{i=1}^{\Gamma_0} K_1^{(i)} \sigma_1^{(i)} \right) \rangle, \quad (3)$$

where $K_1^{(i)} \equiv \beta J_1^{(i)}$ and $\beta \equiv (k_B T)^{-1}$. Here the brackets $\langle \rangle$ denote both the thermal and the configuration averages. If we let Γ be the number of nearest neighbors interacting with a spin σ_0 , then the distribution of Γ is given by

$$P(\Gamma) = \sum_{n=0}^{\Gamma_0} \binom{\Gamma_0}{n} (1-p)^n p^{\Gamma_0-n} \delta(\Gamma - (\Gamma_0 - n)). \quad (4)$$

Now if we expand the function appearing inside the brackets in Eq. (3), in terms of spin products, and then sum over all possible configurations, we obtain

$$\left(1 + \frac{d}{dt} \right) m_0(t) = \left[\sum_{\Gamma=1}^{\Gamma_0} \binom{\Gamma_0-1}{\Gamma-1} p^\Gamma (1-p)^{\Gamma_0-\Gamma} a_\Gamma(K) \right] \times \sum_{i=1}^{\Gamma_0} m_1^{(i)} + g(p, K, t). \quad (5)$$

Here $a_\Gamma(K)$ is the coefficient of the first order term coming from the expansion of the function in terms of products of spin variables, for a particular configuration in which spin σ_0 has Γ interacting nearest neighbors. These coefficients are given by

$$a_\Gamma(K) = \frac{1}{\Gamma 2^{\Gamma-1}} \sum_{n=0}^{n_{\max}} \binom{\Gamma}{n} (\Gamma - 2n) \tanh[(\Gamma - 2n)K], \quad (6)$$

where n_{\max} takes values $\Gamma/2$ for even Γ or $(\Gamma - 1)/2$ in the case of odd Γ . The other term in Eq. (5), $g(p, K, t)$ comes from the higher order spin products. We see that we can write the equation of motion for a spin variable as

$$\left(1 + \frac{d}{dt} \right) m_0(t) = a(p, K) \sum_{i=1}^{\Gamma_0} m_1^{(i)}, \quad (7)$$

where we ignore the higher order terms and define $a(p, K)$ as

$$a(p, K) = \sum_{\Gamma=1}^{\Gamma_0} \binom{\Gamma_0-1}{\Gamma-1} p^\Gamma (1-p)^{\Gamma_0-\Gamma} a_\Gamma(K). \quad (8)$$

If we take the Laplace transform of the equation (7) we obtain the equation of motion for the magnetization of a spin as

$$(1+s) m_0[s] = a(p, K) \sum_{i=1}^{\Gamma_0} m_1^{(i)}. \quad (9)$$

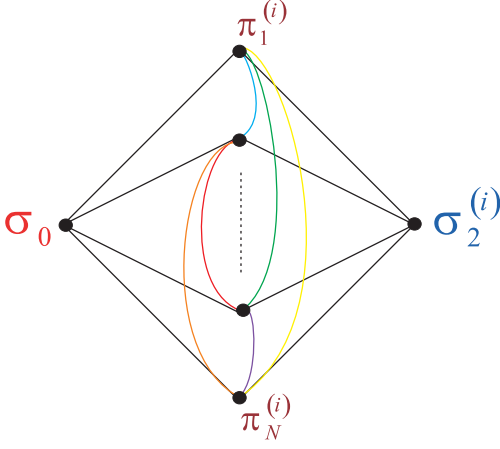


FIG. 6: The cluster in our new scheme which will, in the coarse grained lattice, go to the bond connecting the central spin to its nearest neighbor in the i th direction. The intermediate (“middle”) spins are denoted by $\pi_j^{(i)}$, $j = 1, \dots, N$. This approach preserves the inter-connectivity of the “middle” spins and is thus able to estimate better the number of different paths, or loops, contributing to the spin correlations. (Our figure is in color in the on-line version.)

B. New clustering scheme

In this subsection we will introduce a new type of clustering scheme other than the conventional Migdal-Kadanoff bond moving approach. Since Migdal-Kadanoff bond moving drastically underestimates the number of loops in the system in high dimensions, we need to introduce a new scheme preserving the inter-connectivity of the nodes which will be eventually decimated (see Fig. 6). We will implement the transformation for the scaling parameter $\lambda = 2$.

According to our new scheme, in the i th direction, $i = 1, \dots, \Gamma_0$, between the “corner” spins σ_0 and $\sigma_2^{(i)}$ there exists a cluster containing $N = \lambda^{d-1}$ “middle” spins denoted by $\pi_j^{(i)}$, with $j = 1, 2, \dots, N$, as illustrated in Fig. 6. All the “middle” spins can be connected to the “corner” spins and to the rest of the “middle” spins in the cluster. The “corner” spins will remain after decimation, and may have a maximum number $\Gamma_{0,c} = \Gamma_0 N$ of nearest neighbors. The “middle” spins will be decimated through the last step of the dynamical RG calculations, and the maximum number of nearest neighbors they may have is $\Gamma_{0,m} = N + 1$. We postulate that the bond occupation probability p , and the bond strength J remain invariant after the application of our new type of bond moving scheme, and the interaction between any pair of spins on the cluster obeys the same distribution as in Eq. (2). The distribution of the number of nearest neighbors

is given by

$$P(\Gamma') = \sum_{n=0}^{\Gamma'_{\max}} \binom{\Gamma'_{\max}}{n} (1-p)^n p^{\Gamma'_{\max}-n} \delta(\Gamma' - (\Gamma'_{\max} - n)), \quad (10)$$

where Γ'_{\max} is $\Gamma_{0,c}$ for the “corner” spins and $\Gamma_{0,m}$ for the “middle” spins.

The equation of motion for the expectation value of the j th “middle” spin in the i th direction now becomes,

$$\left(1 + \frac{d}{dt}\right) \langle \pi_j^{(i)} \rangle = \gamma(p, K) \left[m_0 + m_2^{(i)} + \sum_{k \neq j} \langle \pi_k^{(i)} \rangle \right], \quad (11)$$

where $\gamma(p, K)$ comes from the configuration average given by

$$\gamma(p, K) = \sum_{\Gamma'=1}^{\Gamma_{0,m}} \binom{\Gamma_{0,m}}{\Gamma'-1} p^{\Gamma'} (1-p)^{\Gamma_{0,m}-\Gamma'} a_{\Gamma'}(K). \quad (12)$$

If we write down the equation of motion for the expectation value of the “corner” spins we obtain

$$\left(1 + \frac{d}{dt}\right) m_0(t) = A(p, K) \sum_{i=1}^{\Gamma_0} \sum_{j=1}^N \langle \pi_j^{(i)} \rangle, \quad (13)$$

where $A(p, K)$ comes from the configuration average,

$$A(p, K) = \sum_{\Gamma'=1}^{\Gamma_{0,c}} \binom{\Gamma_{0,c}}{\Gamma'-1} p^{\Gamma'} (1-p)^{\Gamma_{0,c}-\Gamma'} a_{\Gamma'}(K). \quad (14)$$

C. Obtaining the dynamical RSRG equations

Now we are ready to perform the decimation. The aim is to rewrite the equation of motion for the “corner” spins in terms of their λ th neighbors. In our case, with $\lambda = 2$, this means obtaining the equation of motion for m_0 in terms of the $m_2^{(i)}$ ’s. For this purpose we will write down all the equations obtained for the “middle” spins $\pi_j^{(i)}$ in the i th direction and sum all the equations. We get

$$\left[1 + \frac{d}{dt} - (N-1)\gamma(p, K)\right] \sum_{j=1}^N \langle \pi_j^{(i)} \rangle = N\gamma(p, K) \left[m_0 + m_2^{(i)} \right]. \quad (15)$$

Thus we obtain the equation of motion for the “middle” spins in the i th direction in terms of the “corner” spin averages m_0 and $m_2^{(i)}$. If we multiply the equation of motion (13) for m_0 by $\left[1 + \frac{d}{dt} - (N-1)\gamma(p, K)\right]$ we obtain

$$\left[1 + \frac{d}{dt} - (N-1)\gamma(p, K)\right] \left(1 + \frac{d}{dt}\right) m_0(t) = A(p, K) \sum_{i=1}^{\Gamma_0} \left[1 + \frac{d}{dt} - (N-1)\gamma(p, K)\right] \sum_{j=1}^N \langle \pi_j^{(i)} \rangle. \quad (16)$$

Using Eq. (15) we get

$$\left[1 + \frac{d}{dt} - (N-1)\gamma(p, K)\right] \left(1 + \frac{d}{dt}\right) m_0(t) = A(p, K) \sum_{i=1}^{\Gamma_0} N\gamma(p, K) \left[m_0 + m_2^{(i)}\right] \quad (17)$$

and

$$\left[\left(1 + \frac{d}{dt}\right)^2 - (N-1)\gamma(p, K) \left(1 + \frac{d}{dt}\right) - N\Gamma_0 A(p, K)\gamma(p, K)\right] m_0(t) = NA(p, K)\gamma(p, K) \sum_{i=1}^{\Gamma_0} m_2^{(i)}. \quad (18)$$

If we ignore the second derivative term we obtain

$$\{[1 - (N-1)\gamma(p, K) - N\Gamma_0 A(p, K)\gamma(p, K)] + [2 - (N-1)\gamma(p, K)] \frac{d}{dt}\} m_0(t) = NA(p, K)\gamma(p, K) \sum_{i=1}^{\Gamma_0} m_2^{(i)}. \quad (19)$$

Now let us write this equation in a familiar form,

$$\left\{1 + \frac{2 - (N-1)\gamma(p, K)}{1 - \gamma(p, K) [N - 1 + N\Gamma_0 A(p, K)]} \frac{d}{dt}\right\} m_0 = \frac{NA(p, K)\gamma(p, K)}{1 - \gamma(p, K) [N - 1 + N\Gamma_0 A(p, K)]} \sum_{i=1}^{\Gamma_0} m_2^{(i)}. \quad (20)$$

Taking the Laplace transform we get

$$\left\{1 + \frac{2 - (N-1)\gamma(p, K)}{1 - \gamma(p, K) [N - 1 + N\Gamma_0 A(p, K)]} s\right\} m_0[s] = \frac{NA(p, K)\gamma(p, K)}{1 - \gamma(p, K) [N - 1 + N\Gamma_0 A(p, K)]} \sum_{i=1}^{\Gamma_0} m_2^{(i)}. \quad (21)$$

We see that the equation of motion (21) is in the same form as Eq. (9). We identify the second term in the curly brackets as the renormalized Laplace variable \tilde{s} . The coefficient in front of the summation appearing on the right-hand side, we identify as the coefficient $a(\tilde{p}, \tilde{K})$, expressed in terms of the renormalized variables \tilde{p} , \tilde{K} . We thus obtain the RG equation for the time from

$$\frac{\tilde{s}}{s} = \frac{2 - (N-1)\gamma(p, K)}{1 - \gamma(p, K) [N - 1 + N\Gamma_0 A(p, K)]} \quad (22)$$

and the implicit RG transformation for K from

$$a(\tilde{p}, \tilde{K}) = \frac{NA(p, K)\gamma(p, K)}{1 - \gamma(p, K) [N - 1 + N\Gamma_0 A(p, K)]} \equiv R(p, K), \quad (23)$$

where $a(p, K)$ is given by Eq. (8). The transformation for the renormalized occupation probability \tilde{p} is found

by calculating the probability $f(p)$ of an unbroken path from the spin σ_0 to $\sigma_2^{(i)}$ through the cluster in the i th direction, and is thus independent from K . Thus, the fixed point value for the occupation probability satisfies

$$p^* = f(p^*). \quad (24)$$

Note that this implies that at each stage of the distribution, the distribution of the bond strengths is replaced by a distribution of the initial binary form, Eq.(2), with the renormalised parameters \tilde{p} and \tilde{K} . [25] This may hide from view certain features of the random fixed point associated with the full distribution. [17, 18]

The fixed point of the dynamical RG transformation for K is found from

$$a(p^*, K^*) = R(p^*, K^*), \quad (25)$$

where p^* , found from Eq. (24), should be substituted. We can evaluate the correlation critical exponent ν from

$$\left.\frac{d\tilde{K}}{dK}\right|_{p^*, K^*} = \left[\frac{\partial R(p, K)}{\partial K} / \frac{\partial a(\tilde{p}, \tilde{K})}{\partial \tilde{K}}\right] \Big|_{p^*, K^*} = \lambda^{-\nu}, \quad (26)$$

and the dynamical critical exponent z is given by

$$\left.\frac{\tilde{s}}{s}\right|_{p^*, K^*} = \lambda^z. \quad (27)$$

III. RESULTS AND DISCUSSION

In the foregoing we have presented the generalized dynamical RSRG framework for the kinetic Ising model on diluted d -dimensional lattices with a random number of nearest neighbors, motivated by an interest in the scaling behaviour of relaxation times on random networks.

For the case with no bond dilution, we calculated the correlation length critical exponent ν and dynamical critical exponent z with our new scheme of clustering in d -dimensional hypercubic lattices and found that ν converges to 0.63 and z converges to 1.6 for large d values as shown in Figs. (3,4). The numerical values are given in Table 1. These results are much better than those obtained by the conventional Migdal-Kadanoff bond moving scheme which is shown in Figs. (2, 1), respectively. Note that, here, just as for the conventional Migdal-Kadanoff bond moving scheme, these results for the critical point and the correlation exponent differ from those found directly from the fixed point of a RSRG transformation obtained by decimating the middle spins in the cluster shown in Fig. 6. We denote the latter scheme as the ‘‘static approach’’ and have reported the results for the correlation length exponent found in this way under ν_{static} .

Our new scheme yields dynamical critical exponent values $z = 2.13$ and $z = 2.09$ in two and three dimensions, as well as the percolation exponent ν_p . We report

TABLE I: Our results for dynamical critical exponent z and correlation critical exponent ν with respect to space dimension d at the pure Ising fixed point.

d	z	ν_{dynamic}	ν_{static}
2	2.13	0.49	1.15
3	2.09	0.51	0.82
4	1.99	0.54	0.72
5	1.88	0.57	0.68
6	1.77	0.59	0.65
7	1.70	0.61	0.64
8	1.65	0.62	0.64
11	1.60	0.63	0.63

TABLE II: The fixed points and the critical exponents in $d = 2$ and $d = 3$. The first value of p shows the pure Ising fixed point, the second one shows the percolation fixed point for each dimension d .

d	p	K^*	ν_p	ν_{dynamic}	α_{dynamic}	z
2	1	0.27	–	0.49	1.03	2.13
	0.5	0.82	1.43	0.48	1.04	2.16
3	1	0.12	–	0.51	0.46	2.09
	0.16	–	1.01	–	–	–

our results in Table 2. We see that the agreement between the known value of $\nu_p = 4/3$ in two dimensions is about as good as the result in three dimensions, with the best Monte Carlo values being reported as $\nu_p = 0.88$ [26]. The values of the dynamical critical exponents are in very good agreement with recent Monte Carlo results, as summarized in Table 3.

For the bond diluted case, we first computed the RG flows for $d = 2$ and $d = 3$ (See Figs. 7, 8). Due to

TABLE III: Comparison of our results with the known values coming from different approaches. Here dynamical RSRG calculations are written as DRSRG and Monte Carlo studies are denoted by MC.

d	Reference	Method	z
2	Present work	DRSRG	2.13
	Stauffer [7]	MC	2.18
	Nightingale <i>et al.</i> [8]	MC	2.17
	Li <i>et al.</i> [9]	MC	2.13
	Lauritsen <i>et al.</i> [10]	MC	2.13 ± 0.02
	Adler <i>et al.</i> [11]	MC	2.21 ± 0.03
	Droz <i>et al.</i> [6]	DRSRG	1.85
3	Present work	DRSRG	2.09
	Ito <i>et al.</i> [12]	MC	2.06
	Stauffer [7]	MC	2.04
	Lauritsen <i>et al.</i> [10]	MC	2.04 ± 0.03
	Adler <i>et al.</i> [11]	MC	2.08 ± 0.03
	Ito [13]	MC	2.06 ± 0.02
	Droz <i>et al.</i> [6]	DRSRG	1.45
6	Present work	DRSRG	1.77
	Droz <i>et al.</i> [6]	DRSRG	1.02

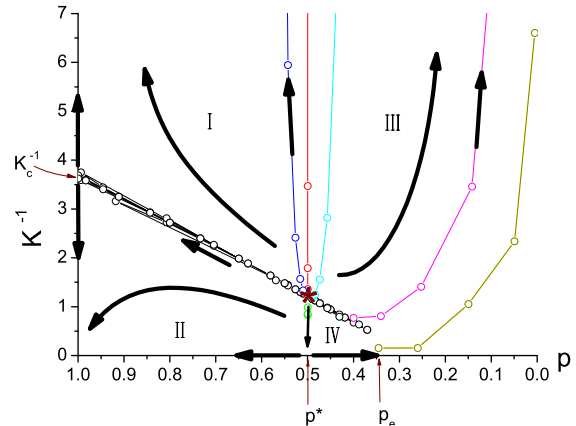


FIG. 7: The phase diagram, $K^{-1} = k_B T/J$ versus p , for $d = 2$. There is an unstable fixed point at $p^* = 0.5$, $(K^*)^{-1} = 1.22$, indicated by * in the figure. The line of points extending to the right of the unstable fixed point is explained in the text. The flow from region IV is to the high temperature, $p = 0$ fixed point. Thus the line from (p^*, T^*) to the percolation fixed point, $(p^*, 0)$ is a first order phase transition line. The critical behaviour on the phase boundary extending from * to the pure Ising fixed point at T_c at $p = 1$, is determined by the latter point. (Our figure is in color in the on-line version.)

the high temperature approximation made in the determination of the RG transformations, these flows are well defined on the disordered side of the separatrix, and also for temperatures less than, but close to, the transition temperatures, but not in the whole ordered region. Nevertheless, their examination is crucial to obtain the phase diagrams correctly.

For $d = 2$, we find that the regions I and II flow, respectively, to the disordered and ordered fixed points at $p = 1$, $T \rightarrow \infty$ and $p = 1$, $T = 0$. The flow on the separatrix itself is to the pure Ising fixed point indicated by T_c on the $p = 1$ line. Note that the line of fixed points of the equation $a(\tilde{p}, K^*) = R(p, K^*)$ extending to the right of (p^*, K^*) and coming down to zero at p_e is not a phase boundary, although it lies close to the separatrix for $p \geq p^*$ and passes through an unstable fixed point at (p^*, K^*) . For $p < p^*$, we find that in both regions III and IV, the flows are to the attractive disordered fixed point at $p = 0$, $T \rightarrow \infty$. The line connecting the unstable fixed point at $p^* = 0.5$, $(K^*)^{-1} = 1.22$, indicated by * in the figure, to the percolation fixed point, $(p^*, 0)$ is therefore a first order phase transition line, separating a region with finite magnetization from one with zero magnetization. This suggests that the unstable fixed point (p^*, K^*) is a tricritical point (TCP), with a first order phase boundary connecting this point to the percolation fixed point $p^* = 0.5$ at $T = 0$. We have checked that along the separatrix, from the unstable disorder fixed point to the pure Ising fixed point, the magnetization is zero. (We have also checked that the mean field-type equation for the

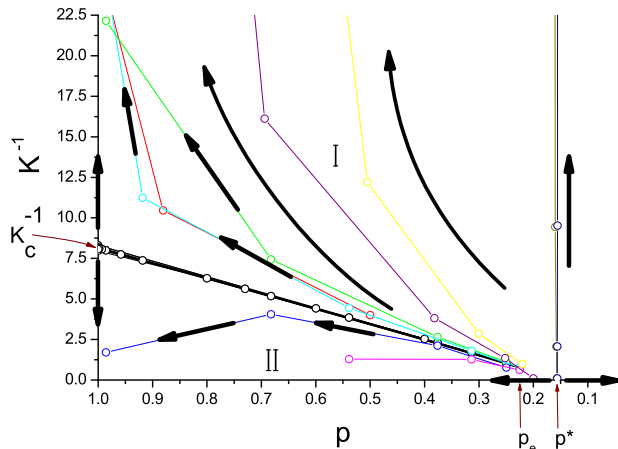


FIG. 8: The phase diagram, $K^{-1} = k_B T/J$ versus p , for $d = 3$. There is no fixed point other than the pure Ising one for non zero temperatures. Thus the critical behaviour of the system is determined by the pure Ising fixed point for finite T . Note that the phase boundary comes down to zero temperature at a concentration p_e which is greater than the percolation fixed point, p^* . (Our figure is in color in the on-line version.)

equilibrium order parameter m_0 , which one may obtain from Eq. (3) by setting all the magnetizations to be the same, and interpreting the brackets as purely configuration averages, gives a second order phase transition in this interval, with the expected value of the order parameter critical exponent $\beta = 0.5$.) The value of ν_{dynamic} and z at the TCP are, 0.48 and 2.16 respectively. (Similar unexpected features have arisen in other phase diagrams obtained via RSRG treatments of systems with random bonds. [27])

For $d = 3$ the dynamical RG results for ν gives, via $\alpha = 2 - d\nu$, once again a positive value for α (although the static result is negative, as can be readily computed from the values in Table 1). However, we now find that there is no K which the RG relation $a(p^*, K^*) = R(p^*, K^*)$ is satisfied. Examining the flow diagram in Fig. 8, we see that the phase separation line comes down to $T = 0$ at some $p_e > p^*$, precluding such a fixed point. The flow in regions I and II are respectively to the disordered and ordered fixed points, while on the separatrix it is once more to the pure Ising fixed point. For very low temperatures, near p_e , the details of the phase boundary are not available, due to the same difficulty as we encountered for $d = 2$.

Since Monte Carlo simulations are plagued by

crossover effects along critical lines, we also computed effective critical exponents z_{eff} along the critical line. For each given p along this line, we solved for a p -dependent fixed point of K under the transformation in Eq. (23) which now becomes $a(f(p), K^*) = R(p, K^*)$. We then substitute p and $K^*(p)$ in Eq. (22) and evaluate z_{eff} from $(\tilde{s}/s)_{p, K^*} = \lambda^{z_{\text{eff}}}$. We find that for $d = 2$, z_{eff} first increases from 2.13 at $p = 1$ till 2.25 at $p = 0.75$ and then decreases to 2.01 at p_e . For $d = 3$ the dependence on p is again non-monotonic, starting from 2.09 at $p = 1$, increasing to 2.69 at $p = 0.4$ and decreasing to 2.54 at p_e .

The calculation of the dynamical critical exponent z for the bond (or site) diluted quenched random Ising model are currently the subject of numerical studies. Recent Monte Carlo simulations for the dynamical critical exponent z for the bond diluted quenched random Ising model have only yielded an effective exponent, z_{eff} , varying between 0.59 to 0.27 along the critical line. [28] These values are markedly lower than the values found here.

For $d \geq 4$, considering either the static or the dynamic values of the correlation length exponent in Table 1, we find a negative specific heat exponents from the hyperscaling relation $\alpha = 2 - d\nu$. This suggests, although not conclusively [21], that on all these lattices, the pure Ising fixed point will be attractive within this approach. Under dilution, the critical behaviour on the second order phase boundary will be determined by the pure Ising fixed point. In Table 1 we also display the dynamical critical exponent z at the pure Ising fixed point for these values of d .

It should be recalled that the exponents we have reported so far are *exact* on hierarchical lattices [14, 15] generated by iterative replacement of each line in the cluster shown in Fig. 6, by the cluster itself. We may define an effective dimension of this hierarchical lattice as being given via $2^{d_{\text{eff}}-1} = N$, where N is the number of intermediate spins in the cluster in Fig. 6, and where we have taken the scale transformation factor to be $\lambda = 2$. For the undiluted case, we obtain a network with a degree distribution which is power law such that $n(\Gamma) \sim \Gamma^{-\gamma}$, where $\gamma = 1 + \ln[2 + (N-1)/2]/\ln N$. We may now construct random hierarchical lattices by randomly diluting each cluster, with a uniform bond occupation probability p , to get the asymptotic degree distribution $\sim \exp[-(1-p)\Gamma]/\Gamma!$ for small p . From the discussion above, we conclude that for effective dimension $d \geq 4$, the pure Ising behaviour will be observed on the critical line for $T > 0$, and $p > p_e(d)$ on these hierarchical lattices.

Acknowledgements

AE would like to gratefully acknowledge partial support from the Turkish Academy of Sciences.

[1] M. Suzuki, K. Sogo, I. Matsuba, H. Ikeda, T. Chikama, and H. Takano, Prog. of Theor. Phys. **61**, 864 (1979).

[2] S. N. Dorogovtsev and J. F. F. Mendes, Adv. Phys. **51**, 1079 (2002).

- [3] A. A. Migdal, Zh. Eksp. Theor. Fiz. **69**, 1457 (1975).
- [4] L. P. Kadanoff, Ann. of Phys. **100**, 359 (1976).
- [5] M. Droz, Phys. Lett. A **73**, 407 (1979).
- [6] M. Droz and A. Malaspinas, J. Phys. C **13**, 4365 (1980).
- [7] D. Stauffer, Physica A **244**, 344 (1997).
- [8] M. P. Nightingale and H. W. Blöte, Phys. Rev. Lett. **76**, 4548 (1996).
- [9] Z. B. Li, L. Schülke, and B. Zheng, Phys. Rev. Lett. **74**, 3396 (1995).
- [10] K. B. Lauritsen and N. Ito, Physica A **202**, 224 (1994).
- [11] C. Mülker, D. W. Heerman, J. Adler, M. Gofman, and D. Stauffer, Physica A **193**, 540 (1993).
- [12] N. Ito, Y. Ozeki, in D. P. Landau, S. P. Lewis, H. -B. Schüttler (Eds.), *Computer Simulation Studies in Condense Matter Physics*, (Springer, Heidelberg, 2001), Vol. XII, pp. 175, cited in N. Ito, Y. Ozeki, Physica A **321**, 262 (2003).
- [13] N. Ito, Physica A **192**, 604 (1993).
- [14] A. N. Berker and S. Ostlund, J. Phys. C **12**, 4961 (1979).
- [15] M. Kaufman and R. B. Griffiths, Phys. Rev. B **24**, 496 (1981).
- [16] M. Droz and A. Malaspinas, Helv. Phys. Acta **53**, 241 (1980).
- [17] D. Andelman and A.N. Berker, Phys. Rev. B **29**, 2630 (1984).
- [18] S. Wiseman and E. Domany, Phys. Rev. E **58**, 2938 (1998).
- [19] H. G. Ballestros, L. A. Fernández, L. Martin-Mayor, A. Muñoz Sudupe, G. Parisi, and J.J. Ruiz-Lorenzo, Phys. Rev. B **58**, 2740 (1998) and references therein.
- [20] A. B. Harris, J. Phys. C **7**, 1671 (1974).
- [21] W. Janke and M. Weigel, Phys. Rev. B **69**, 144208 (2004).
- [22] J.-M. Luck, Europhys. Lett. **24**, 359 (1993).
- [23] A. Efrat and M Schwartz, Phys. Rev. E **62**, 2952 (2000); A. Efrat, Phys. Rev. E **63**, 066112.
- [24] R. J. Glauber, J. Math. Phys. **4**, 294 (1963).
- [25] Y. M. Yeomans and R. B. Stinchcombe, J. Phys. C **12**, 347 (1979).
- [26] D. Stauffer and A. Aharony, *Introduction to Percolation Theory*, (Taylor and Francis, London, 1994), pp.52.
- [27] A. Falicov and A. N. Berker, Phys. Rev. Lett. **76**, 4380 (1996).
- [28] P. E. Berche, C. Chatelain, B. Berche, and W. Janke, Eur. Phys. J. B **38**, 463 (2004) and references therein.